1521-0103/383/1/44–55$35.00
THE JOURNAL OF PHARMACOLOGY AND EXPERIMENTAL THERAPEUTICS
Copyright © 2022 by The American Society for Pharmacology and Experimental Therapeutics
dx.doi.org/10.1124/jpet.122.001268
J Pharmacol Exp Ther 383:44–55, October 2022

The Journal of PHARMACOLOGY And Experimental Therapeutics

Murine Central Nervous System and Bone Marrow Distribution of the Aurora A Kinase Inhibitor Alisertib: Pharmacokinetics and Exposure at the Sites of Efficacy and Toxicity

Ju-Hee Oh[1], Erica A. Power[1], Wenjuan Zhang, David J. Daniels, and William F. Elmquist

Brain Barriers Research Center, Department of Pharmaceutics, College of Pharmacy, University of Minnesota, Minneapolis, Minnesota (J-H.O., W.Z., W.F.E.); Department of Neurologic Surgery, Mayo Clinic, Rochester, Minnesota (E.A.P., D.J.D.); and Mayo Clinic Graduate School of Biomedical Sciences, Mayo Clinic, Rochester, Minnesota (E.A.P.)

Received April 12, 2022; accepted August 1, 2022

ABSTRACT

Important challenges in developing drugs that target central nervous system (CNS) tumors include overcoming barriers for CNS delivery and reducing systemic side effects. Alisertib, an aurora A kinase inhibitor, has been examined for treatment of several CNS tumors in preclinical and clinical studies. In this study, we investigated the distribution of alisertib into the CNS, the site of efficacy for brain tumors, and into the bone marrow, the site of dose-limiting toxicity leading to myelosuppression. Mechanisms influencing site-specific distribution, such as active transport mediated by the efflux proteins, p-glycoprotein (P-gp) and breast cancer resistance protein (Bcrp), were examined. Alisertib exposure to the brain in wild-type mice was less than 1% of that in the plasma, and was evenly distributed throughout various brain regions and the spinal cord. Studies using transporter knockout mice and pharmacological inhibition show that alisertib CNS distribution is influenced by P-gp, but not Bcrp. Conversely, upon systemic administration, alisertib distribution to the bone marrow occurred rapidly, was not significantly limited by efflux transporters, and reached higher concentrations than in the CNS. This study demonstrates that, given an equivalent distributional driving force exposure in plasma, the exposure of alisertib in the brain is significantly less than that in the bone marrow, suggesting that targeted delivery may be necessary to guarantee therapeutic efficacy with minimal risk for adverse events.Therefore, these data suggest that, to improve the therapeutic index when using alisertib for brain tumors, a localized regional delivery, such as convection-enhanced delivery, may be warranted.

SIGNIFICANCE STATEMENT

The CNS penetration of alisertib is limited with uniform distribution in various regions of the brain, and P-gp efflux is an important mechanism limiting that CNS distribution. Alisertib rapidly distributes into the bone marrow, a site of toxicity, with a greater exposure than in the CNS, a possible site of efficacy. These results suggest a need to design localized delivery strategies to improve the CNS exposure of alisertib and limit systemic toxicities in the treatment of brain tumors.

Introduction

A prerequisite for the treatment of central nervous system (CNS) diseases, such as brain tumors, is adequate delivery of a drug into target tissues and to maintain the drug concentration above a minimum therapeutic concentration. This fundamental step, however, acts as a bottleneck on the drug development process, and consequently, insufficient efficacy attributed to poor drug distribution into the CNS is considered a major cause of development failure. A major obstacle of drug penetration into the CNS is the blood-brain barrier (BBB) that impedes influx of endogenous and exogenous compounds into the brain by both physical barriers (e.g., tight junction proteins between brain endothelial cells) and biochemical barriers (e.g., drug efflux transporters) (Banks, 2016; Sarkaria et al., 2018). The constitutive function of the BBB is to protect the brain and to maintain homeostasis of the brain microenvironment. However, with respect to CNS diseases, such as intracranial tumors, the BBB is the object to surmount for achieving a therapeutic drug concentration in lesions (Weiss et al., 2009). Drug distribution into the target tissues could be improved by dose manipulation, but it is highly likely to accompany an increase in systemic or untargeted exposure to the drug, leading to unintended adverse events. Indeed, one of

This work was supported by the State of Minnesota [Minnesota-Mayo Partnership grant ML2020], the National Institutes of Health National Cancer Institute [Grant U01-CA227954], [Grant U54-CA210180], and [Grant U19-CA264362]. E.A.P. would like to acknowledge that this publication was supported by CTSA Grant Number TL1 TR002380 from the National Center for Advancing Translational Science.

No author has an actual or perceived conflict of interest with the contents of this article.

[1]J-H.O. and E.A.P. contributed equally to this work.

dx.doi.org/10.1124/jpet.122.001268.

ABBREVIATIONS: AUC, area under the curve; AUC_{inf}, area under the curve from time zero to infinity; BBB, blood-brain barrier; Bcrp, breast cancer resistance protein; Bcrp1, gene encoding the murine breast cancer resistance protein; CED, convection-enhanced delivery; CNS, central nervous system; K_p, tissue-to-plasma partition coefficient; $K_{p,uu}$, unbound tissue-to-plasma partition coefficient; LC-MS/MS, liquid chromatography-tandem mass spectrometry; *Mdr1*, gene encoding the murine P-glycoprotein; NCA, non-compartmental analysis; P-gp, p-glycoprotein.

Downloaded from jpet.aspetjournals.org at ASPET Journals on April 17, 2024

the reasons for the withdrawal of drug candidates from the drug development process is unintended or severe adverse events. Effective treatment of CNS diseases requires both minimizing side effects and maximizing therapeutic effects.

Alisertib is a selective aurora A kinase inhibitor undergoing clinical trials for several tumors in monotherapy or in combination therapy (Otto and Sicinski, 2017; Mou et al., 2021). Aurora A kinase is a serine/threonine kinase that is a therapeutic target in oncology since it has an essential role in the cell division process, such as spindle assembly and chromosome segregation during mitosis, and is overexpressed in solid and hematologic malignancies. Aurora A kinase inhibitors such as alisertib block cell proliferation at the G2/M phase and, consequently, induce cell cycle arrest followed by apoptosis (Niu et al., 2015). Although alisertib has not yet been approved by FDA for any indications, reports showing its potential for treatment of a variety of cancers, including brain tumors, have been accumulating. For instance, it has been observed that the expression of aurora A kinase is greater in higher grade gliomas (Lehman et al., 2012). In addition, alisertib monotherapy prolongs survival of orthotopic xenografts of patient-derived glioblastoma resistant to bevacizumab (Kurokawa et al., 2017). Interestingly, alisertib affects expression of aurora kinase-related genes which are abnormally expressed in the patient-derived H3K27M cell lines. H3K27M mutation is a somatic mutation occurring in 78% of diffuse midline gliomas that have lysine 27 of histone H3 replaced by methionine. Alisertib also elicits therapeutic benefits in H3K27M tumors in animal models (Wu et al., 2012; Zhang et al., 2018). Currently, a phase 2 clinical trial of alisertib as a single agent and in combination therapy against atypical teratoid rhabdoid tumors is underway (NCT02114229).

Even with potential anticancer efficacy against intracranial tumors, it is important to determine the BBB penetrability and brain distribution of alisertib. A few previous reports indicate that alisertib can cross the BBB to present measurable brain concentrations, but the brain-to-plasma partition coefficient is low. This may be in part due to unfavorable physicochemical properties for brain penetration (Agarwal et al., 2011a; Hill et al., 2015; Sells et al., 2015; Kogiso et al., 2018). Moreover, a major cause limiting CNS distribution of anticancer agents is active efflux transport mediated by p-glycoprotein (P-gp) and breast cancer resistance protein (Bcrp). These transporters, however, may still constrain entry of therapeutics into the tumor cells regardless of the leakiness of the BBB and, as such, attenuate efficacy. Indeed, tumors are guarded by "two layers of efflux transport protection" (Agarwal et al., 2011a), which consists of efflux pumps on brain endothelial cells and tumor cells (de Gooijer et al., 2021; Griffith et al., 2021). Since efflux transporters can impact drug delivery into brain tumors even when the BBB is leaky, understanding the impact of efflux is essential to achieve effective concentrations within both the tumor core and infiltrative regions.

In this study, we investigated the distribution of alisertib into the CNS (i.e., brain and spinal cord) and the bone marrow, sites of efficacy and toxicity, respectively. We also characterized the role of P-gp and Bcrp in CNS and bone marrow distribution of alisertib using a transgenic mouse lacking efflux transporters. These studies conducted in mice suggest that following systemic administration alisertib exposure at the site of efficacy, the CNS, is limited when compared with the exposure at a site of toxicity, the bone marrow, indicating that localized delivery to tumor sites in the brain may be warranted (Fig. 8).

Materials and Methods

Chemicals and Reagents. Alisertib (4-[[9-chloro-7-(2-fluoro-6-methoxyphenyl)-5*H*-pyrimido[5,4-d][2]benzazepin-2-yl]amino]-2-methoxybenzoic acid, purity 99.46%) and MLN8054 (4-[[9-chloro-7-(2,6-difluorophenyl)-5*H*-pyrimido[5,4-d][2]benzazepin-2-yl]amino]benzoic acid, purity 97.90%) were purchased from Selleck Chemicals (Houston, TX). Elacridar (*N*-[4-[2-(6,7-dimethoxy-3,4-dihydro-1*H*-isoquinolin-2-yl) ethyl]phenyl]-5-methoxy-9-oxo-10*H*-acridine-4-carboxamide, purity 98%) was obtained from Toronto Research Chemicals (Toronto, ON, Canada). Captisol was kindly donated from CyDex Pharmaceutical, Inc. (San Diego, CA). All other chemicals were of HPLC-grade or analytical grade and purchased from Thermo Fisher Scientific (Waltham, WA) and MilliporeSigma (St. Louis, MO).

Animals. Pharmacokinetic studies were conducted using an equal number of male and female Friend leukemia virus strain B wild-type, *Mdr1a*/*b*$^{-/-}$ (P-gp knockout), *Bcrp1*$^{-/-}$ (Bcrp knockout), and *Mdr1a*/*b*$^{-/-}$*Bcrp1*$^{-/-}$ (triple knockout of P-gp and Bcrp) mice at the age of 8–16 weeks (Taconic Biosciences, Inc., Germantown, NY). Animals were maintained in a facility accredited by American Association for the Accreditation of Laboratory Animal Care at the Academic Health Center of the University of Minnesota and were housed under a 12 light/12 dark cycle with free access to food and water. Genotyping was regularly conducted to validate gene expression by tail biopsy (Transnetyx, Cordova, TN) since the gene expression and deletion had been confirmed in wild-type and transgenic mice using proteomic analysis (Agarwal et al., 2012). All animal experiments were approved by the University of Minnesota Institutional Animal Care and Use Committee and performed in accordance with the Guide for the Care and Use of Laboratory Animals established by the U.S. National Institutes of Health.

Protein Binding in Mouse Plasma, Brain, and Spinal Cord. Free fraction of alisertib was determined in mouse plasma, brain, and spinal cord by using a rapid equilibrium dialysis device with an 8-kDa molecular weight cutoff cellulose membrane according to the manufacturer's protocol (Thermo Fisher Scientific). Before conducting the protein binding assay, brain and spinal cord from mice were homogenized in 3 volume (w/v) of phosphate-buffered saline. Homogenization was performed using a mechanical homogenizer (THB-01, Omni International, Inc., Kennesaw, GA) at the medium speed setting for 30 seconds. After adjusting pH of blank plasma, brain homogenate, and spinal cord homogenate (i.e., alisertib-free matrix) to 7.4, alisertib solutions in DMSO were added to each blank matrix to a final concentration of 2 and 10 μM containing 0.5% of DMSO. The total drug concentrations were chosen considering the drug concentrations in plasma, brain, and spinal cord in mice after intravenous administration of 5 mg/kg of alisertib. The tissue matrix containing alisertib was added to the insert in the donor chamber, and then phosphate-buffered saline containing 0.5% DMSO was added to the corresponding receiver chamber. The device was covered with sealing tape and incubated at 37°C with shaking at 600 rpm. After 24 hours, samples were collected from both chambers and were kept at -80°C until liquid chromatography-tandem mass spectrometry (LC-MS/MS) analysis. Unbound fraction of alisertib in plasma was calculated by the ratio of drug concentration in the receiver chamber to the drug concentration in the donor chamber. Unbound fraction of alisertib in brain and spinal cord was calculated using the following equation as reported previously (Kalvass and Maurer, 2002):

$$\text{Unbound fraction } (f_u) = \frac{\frac{1}{D}}{\left(\left(\frac{1}{f_{u,\,diluted}}\right) - 1\right) + \frac{1}{D}} \quad (1)$$

Downloaded from jpet.aspetjournals.org at ASPET Journals on April 17, 2024

where D is the dilution factor, in this case 4, and $f_{u,diluted}$ is the ratio of the drug concentration in the receiver chamber to the drug concentration in the donor chamber.

Determination of Blood-to-Plasma Ratio. The blood-to-plasma ratio of alisertib was determined as previously reported with the following modification (Wen et al., 2010). Briefly, alisertib solution in DMSO was spiked into whole blood and plasma to a final concentration of 1 and 10 μM. The drug concentrations were decided considering the plasma concentration of alisertib in mice after intravenous administration of 5 mg/kg of alisertib. Spiked blood and plasma were then incubated at 37°C for 1 hour with shaking at 50 rpm. Whole blood was then centrifuged at 14,000 rpm for 5 minutes at 4°C to separate test plasma. Plasma incubated with alisertib was used as the control plasma, and plasma separated from whole blood after incubation with alisertib was used as the test plasma. Blood-to-plasma ratio was calculated by the ratio of the alisertib concentration in the control plasma to the alisertib concentration in the test plasma.

Pharmacokinetic Study in Wild-Type and Transporter-Knockout Mice. Dosing solution was solubilized in 10% Captisol containing 0.7–0.8% (v/v) 1N NaOH to a final concentration of 1 mg/ml of alisertib. The pH of the dosing solution was checked with a pH indicator strip before administration to assure the pH was close to physiologic. A single intravenous dose of 5 mg/kg alisertib was administered to each genotype through the tail vein followed by serial euthanasia from 5 minutes to 24 hours for wild-type and *Mdr1a/b*$^{-/-}$*Bcrp1*$^{-/-}$ mice, and at 1 hour post dose for *Mdr1a/b*$^{-/-}$ and *Bcrp1*$^{-/-}$ mice using CO_2 gas (n = 4, 2 males and 2 females per each time point). Blood was collected by cardiac puncture using a heparinized syringe followed by centrifugation at 14,000 rpm for 5 minutes at 4°C to separate plasma. The brain was surgically removed from the skull and rinsed with saline. Following removal of superficial meninges by blotting with Kimwipes, the brain was divided into six anatomic regions, including the cortex, cerebellum, hypothalamus + thalamus, midbrain, pons, and medulla. The spinal cord was harvested by hydraulic extrusion from the distal end of a spinal column using a syringe equipped with a 15G needle (Richner et al., 2017). Bone marrow was isolated by centrifugation of femurs and tibias from hind limbs as reported previously (Amend et al., 2016). Plasma and tissue specimens were stored at -80°C until analysis using LC-MS/MS.

Co-Administration of Alisertib with Elacridar. Wild-type and *Mdr1a/b*$^{-/-}$*Bcrp1*$^{-/-}$ mice were randomly divided into two groups. One group, the vehicle-treated group, was dosed 10 ml/kg of elacridar vehicle and the other group, the elacridar-treated group, was dosed 10 mg/kg of elacridar microemulsion in Cremophore EL, Carbitol, and Captex in 6:3:1 ratio. Alisertib was intravenously administered to both groups at 5 mg/kg immediately after intraperitoneal injection of elacridar vehicle or elacridar microemulsion. Dosing regimen of elacridar was determined based on plasma concentration and plasma protein binding of elacridar (Kallem et al., 2012; Sane et al., 2013a). Plasma, whole brain, and spinal cord were collected after 0.25 and 1 hour of administration of alisertib, and then stored at -80°C until LC-MS/MS analysis.

LC-MS/MS Analysis to Measure Plasma and Tissue Concentration. Brain and spinal cord were homogenized in 2 tissue volumes of 5% bovine serum albumin solution (w/v) prior to extraction. Bone marrow was homogenized in 3 tissue volumes of 5% bovine serum albumin solution (w/v) and then diluted in a mixture of blank plasma and 5% bovine serum albumin (1:3, v/v). Fifty microliters of plasma and tissue homogenate were spiked with 5 ng of MLN8054 as an internal standard followed by adding 500 μl of ethyl acetate. The mixture was vortex mixed for 5 minutes at room temperature, and then centrifuged at 14,000 rpm for 5 minutes at 4°C. After freezing at -80°C for 20 minutes, the organic layer on the top was decanted into a microcentrifuge tube and evaporated under nitrogen gas. Dried residue was reconstituted in 100 μl and 50 μl of a mixture of 0.1% formic acid in water and 0.1% formic acid in acetonitrile (30:70, v/v) for plasma and tissues, respectively, and then centrifuged at 14,000 rpm for 5 minutes at 4°C. Supernatant was transferred into a glass vial insert and 5 μl of aliquot was injected into Synergi Polar-RP column (75 × 2 mm, 4 μm, 80 Å; Phenomenex, Torrance, CA) connected to an Agilent 1200 series HPLC system (Agilent Technologies, Santa Clara, CA). The column temperature was maintained at 30°C during analysis. The mobile phase consisted of 0.1% formic acid in water (solvent A) and 0.1% formic acid in acetonitrile (solvent B). A gradient elution was employed as follows at a flow rate of 0.5 ml/min: solvent B was held at 70% for 1 minute, linearly ramped from 70% to 100% in 0.25 minutes, held at 100% for 2 minutes, and brought back down to 70% for 3.5 minutes. A TSQ Quantum Classic and a TSQ Vantage triple stage quadrupole mass spectrometer (Thermo Finnigan, San Jose, CA) equipped with an electrospray ionization source were used to measure plasma concentration and tissue concentration, respectively. The analysis was performed using single reaction monitoring system with the transitions of m/z 519.1 > 328.1 and m/z 477.1 > 316.0 for alisertib and MLN8054, respectively, in positive electrospray ionization mode. The limit of quantifications were 1 ng/ml, 0.2 ng/ml, and 0.1 ng/ml for plasma, brain and spinal cord homogenate, and bone marrow homogenate, respectively. The precision (coefficient of variation less than 15%) and accuracy (relative error less than 15%) were both within acceptable limits.

Correction of the Brain Concentration by Subtracting the Drug Amount in Residual Brain Blood. The alisertib concentration measured in brain homogenate is derived from the concentration of alisertib in the brain tissue and the residual blood in that tissue. This requires that the brain homogenate concentrations be corrected by subtracting the alisertib amount in the cerebral blood from that in the brain homogenate. This is accomplished using the blood-to-plasma ratio and hematocrit.

By definition, a blood-to-plasma ratio in the brain specimen is as follows:

$$R_b = \frac{Drug\ concentration\ in\ blood}{Drug\ concentration\ in\ plasma} = \frac{A_{b,\ brain} / V_{b,\ brain}}{A_{p,\ brain} / V_{p,\ brain}} \quad (2)$$

where R_b, $A_{b,\ brain}$, $V_{b,\ brain}$, $A_{p,\ brain}$, and $V_{p,\ brain}$ are the blood-to-plasma ratio, the drug amount in cerebral blood, the volume of blood in the brain, the drug amount in cerebral plasma, and the volume of plasma in the brain. Given 1.4% of plasma volume of brain weight (Dai et al., 2003), $V_{b,\ brain}$ is calculated by:

$$V_{b,\ brain} = \frac{BW \times 0.014}{1 - Hct} \quad (3)$$

where BW and Hct are the brain weight and the hematocrit, respectively. By rearranging the eq. 2, the $A_{b,\ brain}$ can be calculated by using the following equation:

$$A_{b,\ brain} = R_b \times A_{p,\ brain} \times \frac{V_{b,\ brain}}{V_{p,\ brain}} = R_b \times \frac{BW \times 0.014}{1 - Hct} \times C_p \quad (4)$$

where C_p is the systemic plasma concentration.

The hematocrit (Hct) was estimated to be 0.45 (Bolliger and Everds, 2012). Brain concentrations were calculated by subtracting $A_{b,\ brain}$ from the drug amount in brain homogenate, and then the drug amount in the brain tissue, that does not include the amount of drug in the blood of that tissue, was divided by the brain weight. This method yields the concentration that represents the exposure of the brain tissue to the drug. The spinal cord tissue was evaluated in the same manner.

Pharmacokinetic Calculation. Plasma and tissue concentration-time profiles of alisertib after intravenous administration were analyzed using the non-compartmental analysis (NCA) module of Phoenix WinNonlin version 8.3 (Certara USA, Inc., Princeton, NJ). The terminal rate constant was determined by linear regression using at least three data points in the terminal phase. The pharmacokinetic parameters and metrics, including area under the curve (AUC),

Downloaded from jpet.aspetjournals.org at ASPET Journals on April 17, 2024

clearance, volume of distribution, terminal elimination rate constant, and half-life, reported by Phoenix NCA are presented in Table 2.

The tissue-to-plasma partition coefficient (K_p) was calculated by the ratio of AUC_{inf} of each tissue to AUC_{inf} of plasma. The tissue-to-plasma concentration ratios at 0.25 and 1 hour after administration were calculated by the ratio of the tissue concentration at 0.25 and 1 hour to the plasma concentration at the corresponding time. The tissue-to-plasma partition coefficient of free drug ($K_{p,uu}$) was calculated by multiplying the K_p with the ratio of free fraction of alisertib in tissue to free fraction of alisertib in plasma. Distribution advantage was calculated by dividing K_p of *Mdr1a/b*$^{-/-}$*Bcrp1*$^{-/-}$ mice by K_p of wild-type mice in each brain region, the spinal cord, and the bone marrow.

Statistical Analysis. All experimental data are presented as mean ± standard deviation except for the AUC_{last} which is presented as mean ± standard error calculated by Bailer's method using the Phoenix NCA module (Bailer, 1988). The standard deviation of AUC_{inf} was calculated using Yuan's method as previously reported (Yuan, 1993). A standard deviation of the blood-to-plasma ratio was calculated using propagation of error. An unpaired *t* test was performed to compare protein binding between concentrations and between matrices. The plasma and brain data collected from 4 genotypes after 1 hour of administration were analyzed by one-way ANOVA and two-way ANOVA followed by Tukey's post hoc test, respectively. Data from co-administration study with elacridar were compared by two-way ANOVA followed by Tukey's post hoc test. Normal distribution of data were confirmed with the Shapiro-Wilk test. All statistical comparisons were performed using GraphPad Prism 9.1.1 (GraphPad Software, La Jolla, CA).

Results

Protein Binding and Blood-to-Plasma Ratio. Free fractions of alisertib in plasma, brain, and spinal cord are shown in Table 1. The plasma-free fraction of alisertib is approximately 7-fold higher than free fractions in the brain and spinal cord. Binding of alisertib to the brain was similar to that in the spinal cord, with no statistical difference between brain and spinal cord at both 2 and 10 μM ($p > 0.05$). At 2 μM, free fraction of alisertib was greater when compared with 10 μM in plasma and brain, and the difference was approximately 1.2-fold ($p < 0.05$). Alisertib was stable in plasma, brain homogenate, and spinal cord homogenate for 24 hours at 37°C. The concentrations after a 24 hour-incubation were 90–113% compared with the concentrations in each matrix at time zero (data not shown). The average of free fraction for each matrix (4.2 ± 0.7%, 0.63 ± 0.09%, and 0.61 ± 0.10% in plasma, brain, and spinal cord, respectively) was used to calculate $K_{p,uu}$.

The blood-to-plasma ratio of alisertib was 0.76 ± 0.05 and 0.78 ± 0.08 at 1 and 10 μM with 5 replicates, respectively, and was not statistically different with respect to concentration ($p > 0.05$). The average, 0.77, was used to correct alisertib concentrations in residual tissue blood.

TABLE 1
Protein binding of alisertib in plasma, brain, and spinal cord

	% unbound		
	Plasma	Brain	Spinal cord
2 μM	4.7 ± 0.7	0.69 ± 0.04	0.64 ± 0.13
10 μM	3.8 ± 0.3*	0.57 ± 0.07*	0.58 ± 0.04

Data represent mean ± S.D. (n = 5).
*, $p < 0.05$ compared with 2 μM of the corresponding matrix.

Systemic Exposure and CNS Distribution of Alisertib in Wild-Type and *Mdr1a/b*$^{-/-}$*Bcrp1*$^{-/-}$ Mice. The concentration-time profiles of plasma, 6-brain regions, and spinal cord in wild-type and *Mdr1a/b*$^{-/-}$*Bcrp1*$^{-/-}$ mice resulting from intravenous administration of alisertib at 5 mg/kg are depicted in Figs. 1 and 2. The plasma concentrations declined in a biexponential manner in wild-type mice and the similar concentration-time profiles were observed in *Mdr1a/b*$^{-/-}$*Bcrp1*$^{-/-}$ mice with very similar terminal elimination rate constants (0.17 hour^{-1} and 0.14 hour^{-1} in wild-type and *Mdr1a/b*$^{-/-}$*Bcrp1*$^{-/-}$ mice, respectively). The sampling design was adequate to determine the AUC_{inf} for plasma, brain, and spinal cord, where the extrapolated AUC% was 0.49–2.4%. Clearance, volume of distribution, and terminal half-life were similar between wild-type and *Mdr1a/b*$^{-/-}$*Bcrp1*$^{-/-}$ mice (Table 2).

Concentrations of alisertib in the brain and spinal cord at 24 hours post dose in wild-type mice were below the limit of quantitation or not detected except for the concentration in medulla, which was pooled for the analysis because the specimen from each mouse was limiting. The brain concentration of alisertib was corrected by subtracting alisertib concentrations in residual cerebral blood as described in the Materials and Methods section. The concentration-time profiles and the K_p-time profiles of alisertib in six anatomic brain regions and the spinal cord were superimposable in wild-type and *Mdr1a/b*$^{-/-}$*Bcrp1*$^{-/-}$ mice (Figs. 1–4). $K_{p,\ brain}$ and $K_{p,\ spinal\ cord}$ rapidly increased, peaking at 1 hour after administration and then decreased, reaching a plateau after approximately 8 hours. In mice lacking P-gp and Bcrp, CNS concentrations and K_p of alisertib were significantly greater compared with those in wild-type mice for the duration of the sampling period and the distribution advantage, i.e., the ratio of unbound CNS-to-plasma partition coefficient, in *Mdr1a/b*$^{-/-}$*Bcrp1*$^{-/-}$ mice to that in wild-type mice, was approximately 6 (Figs. 1–4, Table 3). These results suggest that alisertib is a substrate of P-gp and/or Bcrp, leading us to examine whether alisertib is a single substrate for either transporter, or a dual substrate for both, using *Mdr1a/b*$^{-/-}$ and *Bcrp1*$^{-/-}$ mice.

The brain-to-plasma partition coefficients ranged from 0.024 to 0.037 across the brain regions and was 0.020 for spinal cord in wild-type mice, consistent with a previous report (Sells et al., 2015). However, considering the free drug hypothesis that only free drug concentration exerts pharmacological activity (Smith et al., 2010), $K_{p,uu}$, an unbound tissue-to-plasma partition coefficient, and the free concentration in the brain, should be utilized to associate drug distribution into the CNS with therapeutic outcome. The $K_{p,uu}$, which is the corrected K_p using the free fraction of alisertib in plasma and tissue, decreased by 7-fold compared with K_p, in wild-type mice (0.0036–0.0055 and 0.0028 for the brain regions and spinal cord, respectively), indicating that the distribution into the brain from the blood of pharmacologically available alisertib is low (Table 3).

Regional CNS Distribution of Alisertib. Distribution of alisertib into six anatomic brain regions and spinal cord was similar by comparing AUC_{tissue}, K_p, and $K_{p,uu}$ in wild-type and *Mdr1a/b*$^{-/-}$*Bcrp1*$^{-/-}$ mice (Table 2 and 3). Because the CNS regions from wild-type and *Mdr1a/b*$^{-/-}$*Bcrp1*$^{-/-}$ mice were collected by destructive sampling, we statistically compared the regional distribution of alisertib in wild-type, *Mdr1a/b*$^{-/-}$, *Bcrp1*$^{-/-}$, and *Mdr1a/b*$^{-/-}$*Bcrp1*$^{-/-}$ mice at 1 hour post

Downloaded from jpet.aspetjournals.org at ASPET Journals on April 17, 2024

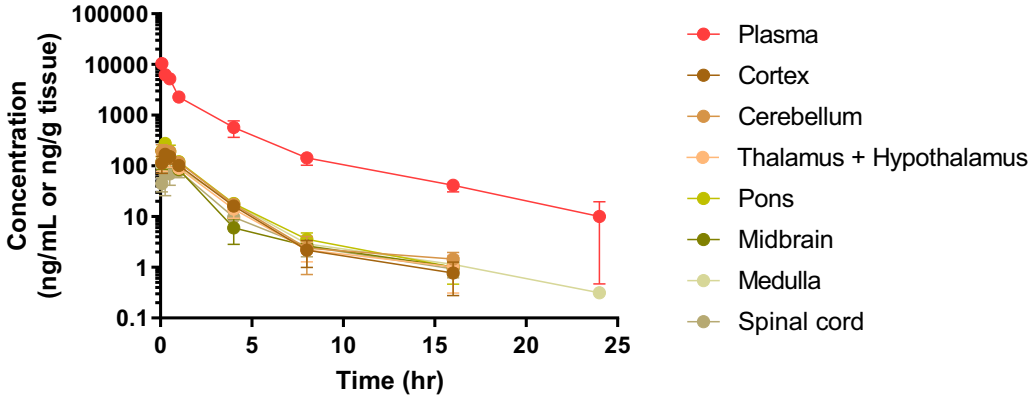

Fig. 1. Plasma and tissue concentration-time profile of alisertib after a single intravenous dose of 5 mg/kg in wild-type mice. The tissue concentration of alisertib was corrected by subtracting alisertib amount in residual tissue blood as described in the Materials and Methods section. Data represent mean ± S.D. (n = 4 at each time point except for medulla. Medulla collected from four mice was pooled and then subjected to analysis).

intravenous administration. The T_{max} of the tissue-to-plasma concentration ratio, which occurred at 1 hour post dose, was chosen as the time point to ascertain the difference in regional distribution among the four mouse genotypes. The tissue concentrations and the tissue-to-plasma concentration ratios were not statistically different across the CNS regions in each genotype (Fig. 5B and Table 4). The p values were 0.7210 and 0.1372 when the tissue concentrations and the tissue-to-plasma concentration ratios, respectively, were compared between brain regions by two-way ANOVA, and no significant pair was observed within the same genotype.

Influence of P-gp and Bcrp on CNS Distribution of Alisertib. The results in wild-type and *Mdr1a/b*$^{-/-}$*Bcrp1*$^{-/-}$ mice suggest that alisertib is a substrate of P-gp and/or Bcrp. To examine if alisertib is a single or dual substrate of efflux transporters, a mouse lacking only P-gp or Bcrp was employed. One hour after intravenous bolus administration, no difference in plasma concentrations of alisertib was observed among four genotypes except for *Mdr1a/b*$^{-/-}$ mice compared with wild-type mice with approximately a 1.3-fold difference (Fig. 5A). The CNS concentrations in *Mdr1a/b*$^{-/-}$ and *Mdr1a/b*$^{-/-}$*Bcrp1*$^{-/-}$ mice were about 8-fold higher compared with those in wild-type and *Bcrp1*$^{-/-}$ mice and the effect of genotype on the CNS concentration of alisertib was significant ($p < 0.001$) (Fig. 5B). When compared the same CNS region between genotypes, the tissue-to-plasma concentration ratios were significantly higher in *Mdr1a/b*$^{-/-}$ and *Mdr1a/b*$^{-/-}$*Bcrp1*$^{-/-}$ mice compared with wild-type mice; approximately 5- and 6-fold, respectively ($p <$ 0.001 for all comparisons). On the contrary, the lack of Bcrp did not affect CNS distribution of alisertib where the tissue-to-plasma concentration ratio was similar between wild-type and *Bcrp1*$^{-/-}$ mice, and between *Mdr1a/b*$^{-/-}$ and *Mdr1a/b*$^{-/-}$*Bcrp1*$^{-/-}$ mice (Table 4). These in vivo results in the CNS suggest that alisertib is a substrate of P-gp, but not a substrate of Bcrp. Given the results in the four genotypes of mice, we conclude that there is no Bcrp influence on CNS distribution of alisertib since there is no compensation between Bcrp and P-gp (Chen et al., 2009; Kodaira et al., 2010; Agarwal et al., 2011).

Elacridar, an Inhibitor of P-gp and Bcrp, Influences CNS Distribution of Alisertib. Elacridar is a potent dual inhibitor of P-gp and Bcrp (Hyafil et al., 1993; Allen et al., 1999; Sane et al., 2013b). We examined the effect of this pharmacological inhibitor on CNS distribution of alisertib after co-dosing with alisertib in wild-type and *Mdr1a/b*$^{-/-}$*Bcrp1*$^{-/-}$ mice. Plasma concentrations of alisertib at 0.25 hours post dose were similar regardless of genotype and elacridar treatment. At 1 hour post dose, plasma concentrations of alisertib of the vehicle-treated group were 1.6-fold higher in *Mdr1a/b*$^{-/-}$*Bcrp1*$^{-/-}$ mice compared with wild-type mice, although they were similar between wild-type and *Mdr1a/b*$^{-/-}$*Bcrp1*$^{-/-}$ mice that did not receive

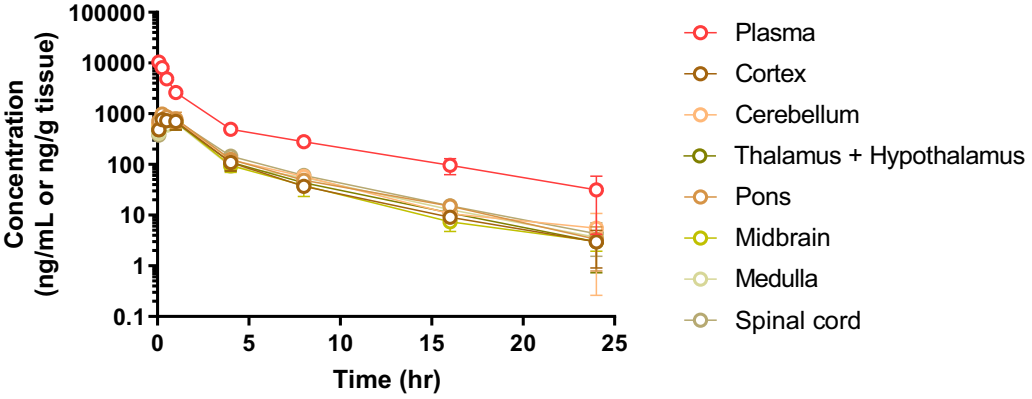

Fig. 2. Plasma and tissue concentration-time profile of alisertib after a single intravenous dose of 5 mg/kg in *Mdr1a/b*$^{-/-}$*Bcrp1*$^{-/-}$ mice. The tissue concentration of alisertib was corrected by subtracting alisertib amount in residual tissue blood as described in the Materials and Methods section. Data represent mean ± S.D. (n = 4 at each time point except for medulla. Medulla collected from four mice was pooled and then subjected to analysis).

Downloaded from jpet.aspetjournals.org at ASPET Journals on April 17, 2024

TABLE 2
Pharmacokinetic parameters of alisertib following a single intravenous dose of 5 mg/kg in wild-type and *Mdr1a/b*$^{-/-}$*Bcrp1*$^{-/-}$ mice

		AUC_{last} μg·hr/ml	AUC_{inf} μg·hr/ml	CL ml/hr/kg	V_{ss} ml/kg	K_e hr^{-1}	$T_{1/2}$ hr
Plasma	Wild-type	12 ± 0	12 ± 0	404	925	0.17	4.2
	Mdr1a/b$^{-/-}$*Bcrp1*$^{-/-}$	14 ± 1	14 ± 1	348	1181	0.14	5.1
Cortex	Wild-type	0.36 ± 0.02	0.36 ± 0.02	—	—	0.24	2.9
	Mdr1a/b$^{-/-}$*Bcrp1*$^{-/-}$	2.4 ± 0.2	2.4 ± 0.2	—	—	0.16	4.4
Cerebellum	Wild-type	0.42 ± 0.02	0.43 ± 0.02	—	—	0.19	3.7
	Mdr1a/b$^{-/-}$*Bcrp1*$^{-/-}$	2.8 ± 0.2	2.8 ± 0.2	—	—	0.16	4.3
Thalamus + Hypothalamus	Wild-type	0.32 ± 0.02	0.33 ± 0.02	—	—	0.20	3.4
	Mdr1a/b$^{-/-}$*Bcrp1*$^{-/-}$	2.4 ± 0.2	2.4 ± 0.2	—	—	0.17	4.1
Pons	Wild-type	0.46 ± 0.02	0.46 ± 0.02	—	—	0.23	3.0
	Mdr1a/b$^{-/-}$*Bcrp1*$^{-/-}$	2.9 ± 0.2	2.9 ± 0.2	—	—	0.18	3.9
Midbrain	Wild-type	0.29 ± 0.02	0.30 ± 0.02	—	—	0.14	4.8
	Mdr1a/b$^{-/-}$*Bcrp1*$^{-/-}$	2.4 ± 0.2	2.4 ± 0.2	—	—	0.17	4.0
Medulla[a]	Wild-type	0.34	0.34	—	—	0.14	5.0
	Mdr1a/b$^{-/-}$*Bcrp1*$^{-/-}$	2.3	2.4	—	—	0.16	4.2
Spinal cord	Wild-type	0.24 ± 0.02	0.24 ± 0.02	—	—	0.18	3.7
	Mdr1a/b$^{-/-}$*Bcrp1*$^{-/-}$	2.7 ± 0.2	2.8 ± 0.2	—	—	0.17	4.2
Bone marrow	Wild-type	3.7 ± 0.1	3.7 ± 0.1	—	—	0.17	4.2
	Mdr1a/b$^{-/-}$*Bcrp1*$^{-/-}$	3.6 ± 0.2	3.7 ± 0.2	—	—	0.13	5.2

Data represent mean ± SE and mean ± S.D. for $AUC_{0\text{-}last}$ and AUC_{inf}, respectively (n = 4 at each time point).
AUC_{inf}, area under the curve from time zero to infinity; AUC_{last}, area under the curve from time zero to the last sampling time point; CL, clearance; K_e, terminal elimination rate constant; $T_{1/2}$, half-life; V_{ss}, volume of distribution at steady state.
[a]Medulla collected from four mice at each time point was pooled, and then subjected to analysis.

the vehicle (Figs. 5A and 6D). It is doubtful that the vehicle of elacridar affected systemic exposure of alisertib, but currently, the reason for this difference is not clear.

The inhibitory effect of elacridar on brain and spinal cord distribution of alisertib was absent at 0.25 hour post dose (Fig. 6, B–C). In wild-type mice, brain and spinal cord distribution of alisertib was markedly increased in the elacridar-treated group compared with the vehicle-treated group after 1 hour of administration, indicating that CNS distribution of alisertib was improved due to inhibition of efflux of alisertib by elacridar treatment (Fig. 6, E–F and Table 5). In *Mdr1a/b*$^{-/-}$*Bcrp1*$^{-/-}$ mice, CNS distribution of alisertib was not different between the vehicle- and elacridar-treated groups (p = 0.9995 and 0.9797 for brain and spinal cord, respectively, at 1 hour post dose), suggesting that elacridar was not able to exhibit inhibitory effect due to lack of P-gp.

Bone Marrow Distribution. Distribution of alisertib into bone marrow in wild-type and *Mdr1a/b*$^{-/-}$*Bcrp1*$^{-/-}$ mice was determined following a single intravenous administration of alisertib at 5 mg/kg to determine if the concentrations at the site of toxicity are associated with function of P-gp and/or Bcrp. The alisertib concentration time-profiles in bone marrow were very similar to those in plasma, with the bone marrow concentrations 3–4 times lower than the plasma concentration in wild-type and *Mdr1a/b*$^{-/-}$*Bcrp1*$^{-/-}$ mice. The elimination rate constants were almost identical between plasma and bone marrow in both genotypes (Fig. 7 and Table 2). Interestingly, alisertib distributed into bone marrow rapidly, and the bone marrow-to-plasma concentration ratio reached a plateau within 5 minutes after intravenous administration. K_p of bone marrow was 0.30 and 0.25 in wild-type and *Mdr1a/b*$^{-/-}$*Bcrp1*$^{-/-}$ mice, respectively, and the bone marrow-to-plasma concentration ratios were also similar in all genotypes after 1 hour of intravenous administration (Tables 3 and 4). Because the amount of bone marrow collected was limiting, the free fraction in bone marrow was not able to be determined, and subsequently, $K_{p,uu}$ was not calculated.

Discussion

Chemotherapy is a necessary component in the treatment of most malignant brain tumors, especially when the tumor is

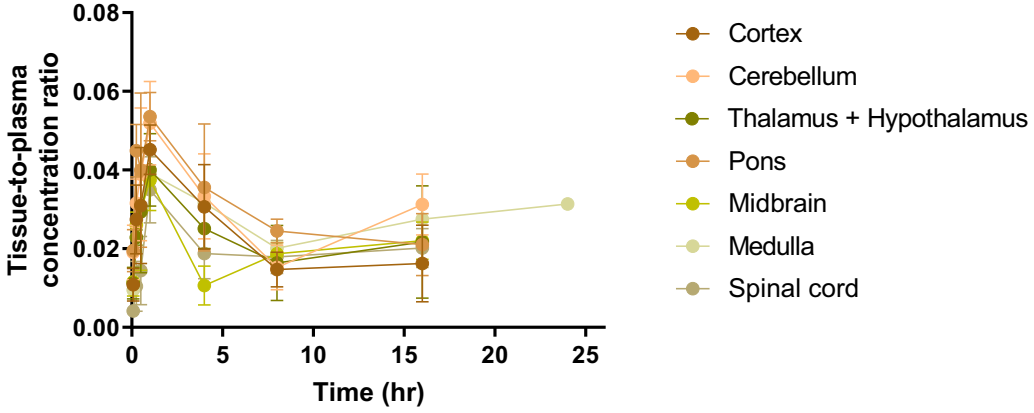

Fig. 3. Tissue-to-plasma concentration ratio-time profile of alisertib after a single intravenous dose of 5 mg/kg in wild-type mice. Data represent mean ± S.D. (n = 4 at each time point except for medulla. Medulla collected from four mice was pooled and then subjected to analysis).

Downloaded from jpet.aspetjournals.org at ASPET Journals on April 17, 2024

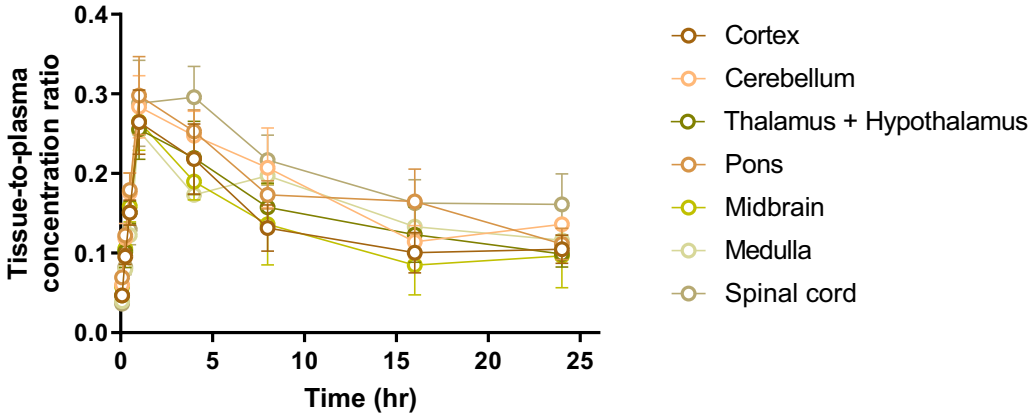

Fig. 4. Tissue-to-plasma concentration ratio-time profile of alisertib after a single intravenous dose of 5 mg/kg in *Mdr1a/b*$^{-/-}$*Bcrp1*$^{-/-}$ mice. Data represent mean ± S.D. (n = 4 at each time point except for medulla. Medulla collected from four mice was pooled and then subjected to analysis).

not amenable to surgical resection and may be resistant to radiotherapy. A critical determinant of the efficacious use of chemotherapy in this context is adequate drug distribution through a heterogeneously intact BBB. Drug delivery leading to efficacy is dependent upon: 1) BBB permeability (including influence of active efflux transport), 2) drug binding in the brain and at the tumor site, and 3) a sufficient retention time, in light of the drug's mechanism of cell kill, at the site of action. Moreover, understanding the relative exposures to sites of action versus sites of toxicity is critical in developing specific dosage regimens with an acceptable therapeutic index. A full appreciation of these parameters for specific drugs in certain types of brain tumor is required for informed clinical trial design.

Efflux transport systems influence drug distribution even in the brain tumor core (de Gooijer et al., 2021; Griffith et al., 2021). We evaluated the brain and spinal cord distribution of alisertib in wild-type and transporter-knockout mice, and these in vivo results show that alisertib is a substrate of P-gp and not Bcrp. Alisertib has a limited CNS penetration in the mouse due in large part to the efflux mediated by P-gp. Importantly for the use of alisertib in brain tumors, its distribution was consistently uniform in different anatomic regions of the brain. This finding also implies an equivalent functional activity of P-gp throughout the different anatomic regions.

Some brain tumors occur in specific brain regions, for example, diffuse midline gliomas in the brainstem/thalamus, while medulloblastomas normally occur around the 4th ventricle. Both are tumor types that are under study for treatment with alisertib (Hill et al., 2015; Zhang et al., 2018). Alisertib is also in a phase 2 study for patients with atypical teratoid rhabdoid tumors (NCT02114229). In this sense, we evaluated CNS distribution of alisertib in six anatomic brain regions (cortex, cerebellum, thalamus and hypothalamus, pons, midbrain, and medulla) and the spinal cord with respect to the function of efflux transporters. K_p and $K_{p,uu}$ of alisertib was consistent across these regions in wild-type mice, suggesting that alisertib distributes uniformly throughout the CNS regions. Moreover, a uniform increase of K_p in mice lacking P-gp implies that there is no functional difference in P-gp activity from one CNS region to another. This finding is in line with a previous report in which the brain distribution of colchicine, a P-gp substrate, did not match in different brain areas after in situ brain perfusion, but it was correlated to the regional flow rate of perfusate. Importantly, the brain distribution of colchicine was significantly increased in all brain regions studied by including PSC833 or elacridar in the perfusate (Youdim et al., 2004). Also, positron emission tomography scans of verapamil and *N-desmethyl*-loperamide, which are typical substrates of P-gp, in the brain in a human and a non-human primate, respectively, showed a uniform function of P-gp across different brain regions (Liow et al., 2009; Eyal et al., 2010). The other reason for uniform distribution of alisertib in the brain could be explained by the uniform expression of P-gp in various mouse

TABLE 3
Tissue-to-plasma partition coefficient of alisertib following a single intravenous administration of 5 mg/kg in wild-type and *Mdr1a/b*$^{-/-}$*Bcrp1*$^{-/-}$ mice

	Wild-type		*Mdr1a/b*$^{-/-}$*Bcrp1*$^{-/-}$		
	K_p	$K_{p,uu}$	K_p	$K_{p,uu}$	Distribution advantage
Cortex	0.029	0.0043	0.17	0.025	5.79
Cerebellum	0.035	0.0052	0.20	0.029	5.63
Thalamus + Hypothalamus	0.026	0.0039	0.17	0.025	6.46
Pons	0.037	0.0055	0.20	0.030	5.39
Midbrain	0.024	0.0036	0.17	0.025	6.99
Medulla[a]	0.028	0.0041	0.16	0.024	5.90
Spinal cord	0.020	0.0028	0.19	0.028	9.79
Bone marrow	0.30	—	0.25	—	0.84

K_p was calculated using AUC from time zero to infinity after destructive sampling from four mice at each time point.
K_p, tissue-to-plasma partition coefficient; $K_{p,uu}$, unbound tissue-to-plasma partition coefficient.
[a]Medulla collected from four mice at each time point was pooled, and then subjected to analysis.

Downloaded from jpet.aspetjournals.org at ASPET Journals on April 17, 2024

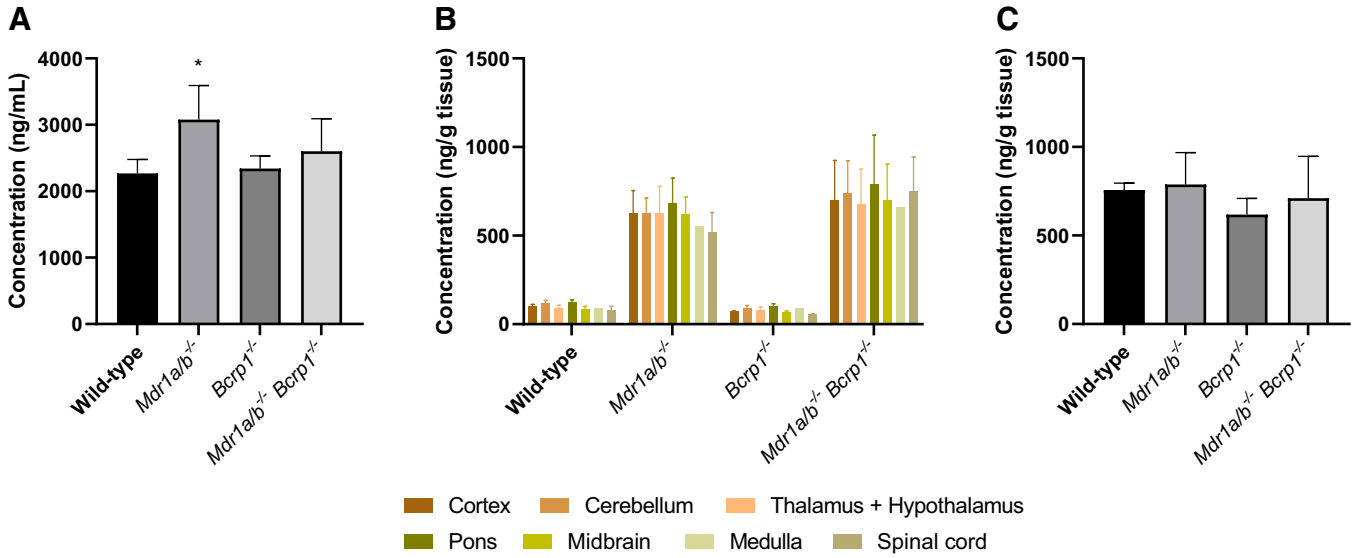

Fig. 5. Alisertib concentrations in plasma (A), CNS (B), and bone marrow (C) at 1 hour post dose following a single intravenous administration of 5 mg/kg in wild-type, *Mdr1a/b*$^{-/-}$, *Bcrp1*$^{-/-}$, and *Mdr1a/b*$^{-/-}$*Bcrp1*$^{-/-}$ mice. The CNS concentration of alisertib was corrected by subtracting alisertib amount in residual tissue blood as described in the Materials and Methods section. *, $p < 0.05$ compared with wild-type mice using one-way ANOVA followed by Tukey's post hoc test. Data represent mean ± S.D. ($n = 4$ at each time point except for medulla. Medulla collected from four mice was pooled and then subjected to analysis).

brain regions. mRNA and protein abundance of P-gp measured in the homogenates of cortex, striatum, midbrain, and hippocampus were similar (You et al., 2019). However, considering P-gp exists in the cerebral endothelium, the region-specific expression determined from isolated brain microvessels could be performed for a more precise interpretation.

In addition to the activity and expression of efflux transporters, other contributors affecting the CNS distribution of some drugs include the cerebral blood flow to different brain areas as described above for colchicine distribution. Differences of regional distribution of flavonoids and steroids were also associated with regional flow in the brain (Youdim et al., 2004; Chugh et al., 2009; Qaiser et al., 2017). The uniform distribution of alisertib in wild-type mice, the uniform increase in distribution in *Mdr1a/b*$^{-/-}$ and *Mdr1a/b*$^{-/-}$*Bcrp1*$^{-/-}$ mice, and the similar distribution between wild-type and *Bcrp1*$^{-/-}$ mice indicate alisertib brain distribution is permeability rate limited with P-gp-mediated efflux at the BBB a major determinant of distribution from blood to the brain.

In addition to the BBB penetrability, variable tissue composition, such as in lipids and proteins, could be another factor that determines distribution of active drug in CNS areas. The lipid content varies between brain regions in rodents, with the highest in the medulla and the lowest in the cortex (Chavko et al., 1993). In humans, the lipid composition is different between brain regions and also between different age groups (Söderberg et al., 1990). Given that the content of phospholipids and neutral lipids affected intracellular drug bioavailability by influencing free drug concentrations and lysosomal pH, respectively, in in vitro experiments, lipid composition and content could be predicted to affect the regional exposure to drugs in the CNS (Treyer et al., 2018). Considering the high lipophilicity of alisertib (log $P = 5$), it could be postulated that the brain distribution of alisertib is affected by different lipid compositions and contents across the brain regions. However, the lipid binding of alisertib is currently unknown. Although $K_{p,uu}$ of alisertib was similar in different CNS regions in mice, it is worthwhile to take lipid binding into account to predict the free drug concentration of alisertib in human brain or tumor tissues. As for the protein composition, it is known that tight junction proteins are more expressed in the white matter than the gray matter (Nyúl-Tóth et al., 2016). In light of the primary function of the tight junction expressed in the CNS, the entry of drugs into the white matter regions would be more restricted than that into the gray matter regions (Daniel et al., 2001). In

TABLE 4

Tissue-to-plasma concentration ratio of alisertib at 1 hour post dose following a single intravenous administration of 5 mg/kg in wild-type, *Mdr1a/b*$^{-/-}$, *Bcrp1*$^{-/-}$, and *Mdr1a/b*$^{-/-}$*Bcrp1*$^{-/-}$ mice

	Wild-type	*Mdr1a/b*$^{-/-}$	*Bcrp1*$^{-/-}$	*Mdr1a/b*$^{-/-}$*Bcrp1*$^{-/-}$
Cortex	0.045 ± 0.006	0.20 ± 0.03***	0.031 ± 0.001	0.26 ± 0.04***
Cerebellum	0.052 ± 0.011	0.20 ± 0.03***	0.038 ± 0.005	0.28 ± 0.04***
Thalamus + Hypothalamus	0.040 ± 0.009	0.20 ± 0.05***	0.033 ± 0.009	0.26 ± 0.04***
Pons	0.054 ± 0.006	0.22 ± 0.04***	0.043 ± 0.011	0.30 ± 0.05***
Midbrain	0.037 ± 0.008	0.20 ± 0.03***	0.028 ± 0.004	0.27 ± 0.04***
Medulla[a]	0.039	0.18	0.039	0.25
Spinal cord	0.035 ± 0.008	0.17 ± 0.03***	0.023 ± 0.002	0.29 ± 0.05***
Bone marrow	0.34 ± 0.03	0.25 ± 0.04	0.26 ± 0.02	0.27 ± 0.06

Data represent mean ± S.D. (n = 4).
***, $p < 0.001$ compared with wild-type mice.
[a]Medulla collected from four mice at each time point was pooled and then subjected to analysis.

Downloaded from jpet.aspetjournals.org at ASPET Journals on April 17, 2024

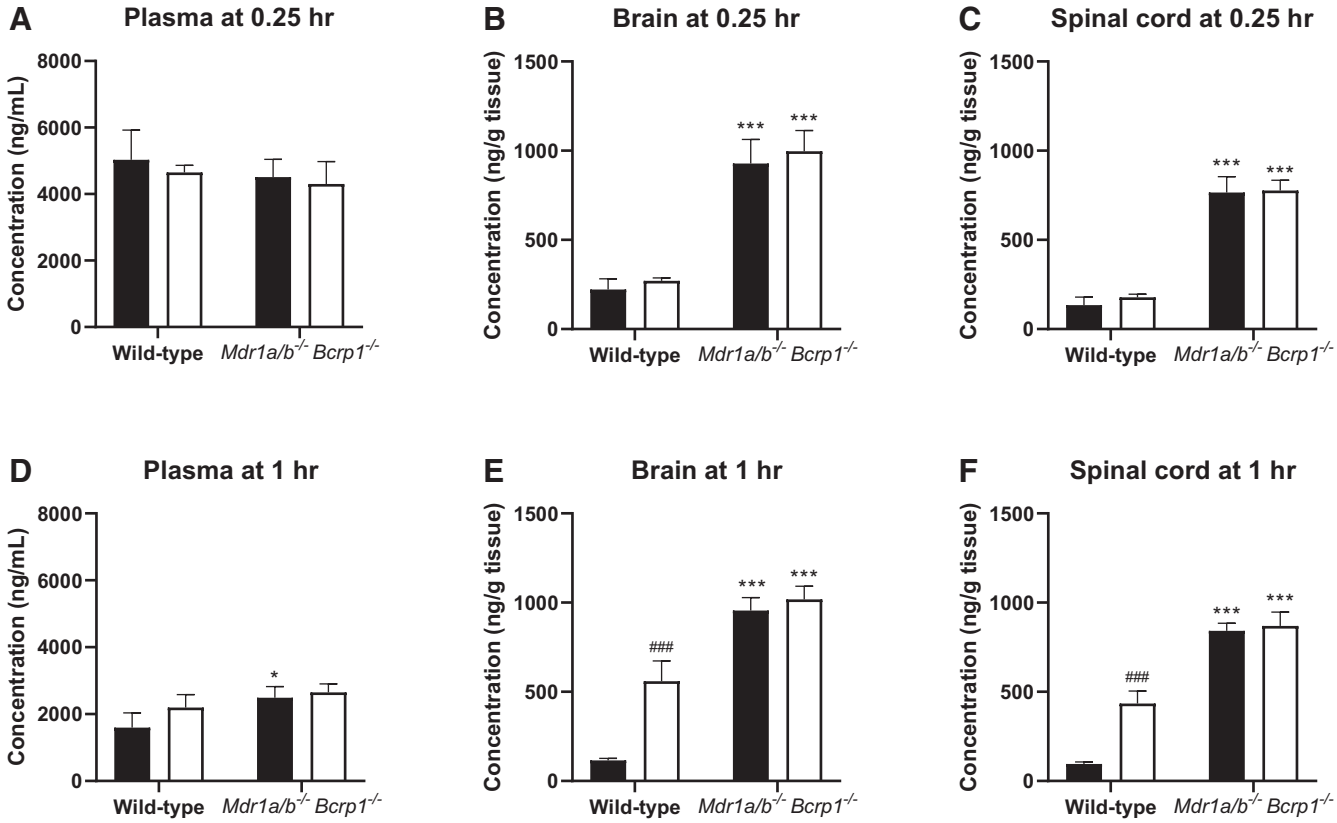

Fig. 6. Alisertib concentrations in plasma (A and D), brain (B and E), and spinal cord (C and F) at 0.25 hours (A, B, and C) and 1 hour post dose (D, E, and F) following co-administration of a single intravenous dose of alisertib (5 mg/kg) and a single intraperitoneal dose of elacridar (10 mg/kg) in wild-type and *Mdr1a/b*$^{-/-}$*Bcrp1*$^{-/-}$ mice. The closed and open bar represent the vehicle- and elacridar-treated group, respectively. The tissue concentration of alisertib was corrected by subtracting alisertib amount in residual tissue blood as described in the Materials and Methods section. *, $p < 0.05$ and ***, $p < 0.001$ compared with the corresponding wild-type mice. ###, $p < 0.001$ compared with the corresponding vehicle-treated group. Statistical analysis was performed by two-way ANOVA followed by Tukey's post hoc test. Data represent mean ± S.D. ($n = 4$).

this study, we did not distinguish the gray and white matter when dissecting the CNS regions, so it is difficult to compare the effect of the expression of tight junctional proteins on CNS distribution of alisertib. Nevertheless, our results inform that alisertib is available evenly in whole brain regions and spinal cord.

P-gp and Bcrp are the major efflux transporters expressed in the CNS. Thus, determining if a drug candidate targeting CNS disease is a substrate of P-gp and Bcrp is essential in the drug development process (Agarwal et al., 2011a). Previously, Michaelis et al. investigated whether P-gp and BCRP was involved in transporting alisertib into neuroblastoma cells by measuring the IC_{50} with the MTT assay. That study indicated that alisertib is not exported by P-gp nor BCRP; however, their interpretation of the results for P-gp needs clarification. Indeed, the results showed that the IC_{50} of alisertib is not significantly changed with high expression of ABCB1, encoding P-gp in humans (Michaelis et al., 2014, 2015). In contrast, our results in wild-type and transporter knockout mice suggest that alisertib is a substrate of P-gp, but not of Bcrp. These results are supported by the previous report that suggests alisertib is a P-gp substrate, not only by comparing accumulation of alisertib in Caco-2 cells in the presence and absence of verapamil, but also by showing higher brain uptake of [^{11}C]-alisertib in P-gp knockout mice compared with wild-type mice (Goos et al., 2016). Recently, it was demonstrated that alisertib was transported by ABCB1 by the bidirectional study in a MDCKII-ABCB1 transfected cell line (Vagiannis et al., 2022).

TABLE 5
Tissue-to-plasma concentration ratio of alisertib at 0.25 hours and 1 hour post dose following co-administration of a single intravenous dose of alisertib (5 mg/kg) and a single intraperitoneal dose of elacridar (10 mg/kg) in wild-type and *Mdr1a/b*$^{-/-}$*Bcrp1*$^{-/-}$ mice

		Brain		Spinal cord	
		Vehicle	Elacridar	Vehicle	Elacridar
Wild-type	0.25 hr	0.046 ± 0.020	0.058 ± 0.005	0.028 ± 0.013	0.038 ± 0.005
	1 hr	0.075 ± 0.016	0.27 ± 0.10$^{\#\#}$	0.063 ± 0.013	0.21 ± 0.07$^{\#\#}$
Mdr1a/b$^{-/-}$*Bcrp1*$^{-/-}$	0.25 hr	0.21 ± 0.03**	0.24 ± 0.07***	0.17 ± 0.02***	0.19 ± 0.04***
	1 hr	0.39 ± 0.07***	0.39 ± 0.01	0.34 ± 0.04***	0.33 ± 0.03*

Data represent mean ± S.D. (n = 4).
*$p < 0.05$, **$p < 0.01$, and ***$p < 0.001$ compared with the corresponding wild-type mice.
$^{\#\#}p < 0.01$ compared with the corresponding vehicle-treated group.

Downloaded from jpet.aspetjournals.org at ASPET Journals on April 17, 2024

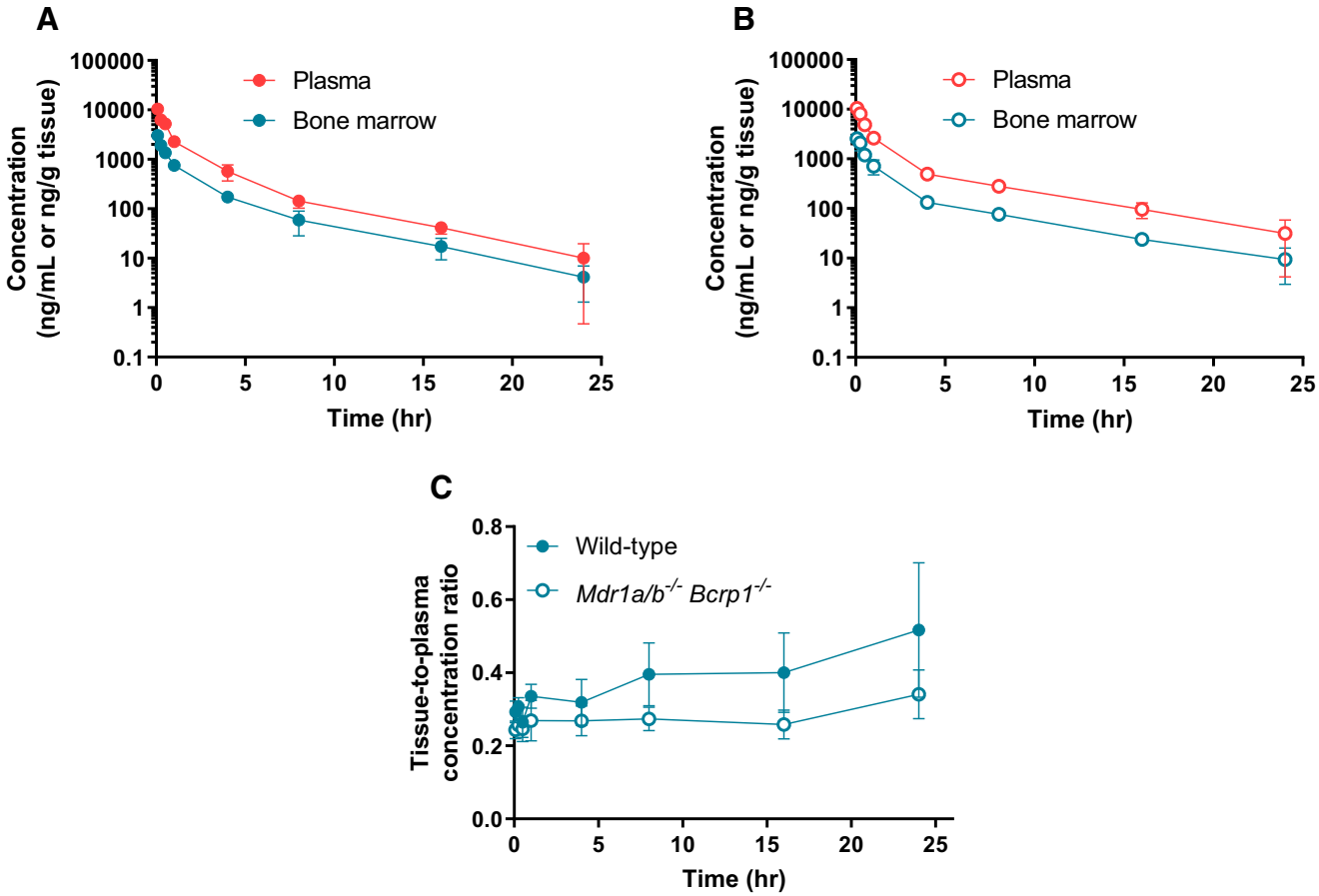

Fig. 7. Plasma and bone marrow concentration-time profiles of alisertib after a single intravenous dose of 5 mg/kg in wild-type (A) and *Mdr1a/b*$^{-/-}$ *Bcrp1*$^{-/-}$ mice (B) and bone marrow-to-plasma concentration ratio-time profile (C). Plasma concentrations are the same as in Figs. 1 and 2. Data represent mean ± S.D. (n = 4 at each time point).

As Figs. 1 and 2 show, the plasma concentration-time profile of alisertib is superimposable between wild-type and *Mdr1a/b*$^{-/-}$*Bcrp1*$^{-/-}$ mice. These results indicate that the transport systems are likely not impacting the systemic clearance of alisertib. In rodents, alisertib is metabolized by glucuronidation, hydroxylation, and oxidation, with a moderate hepatic extraction ratio across species (Yang et al., 2014). Also, in humans, approximately 90% of orally dosed alisertib was excreted through the fecal route, with approximately 26% of the unchanged drug excreted in the feces, and the urinary excretion was minimal (Pusalkar et al., 2020). These reports suggest that the major pathway of elimination is metabolism rather than

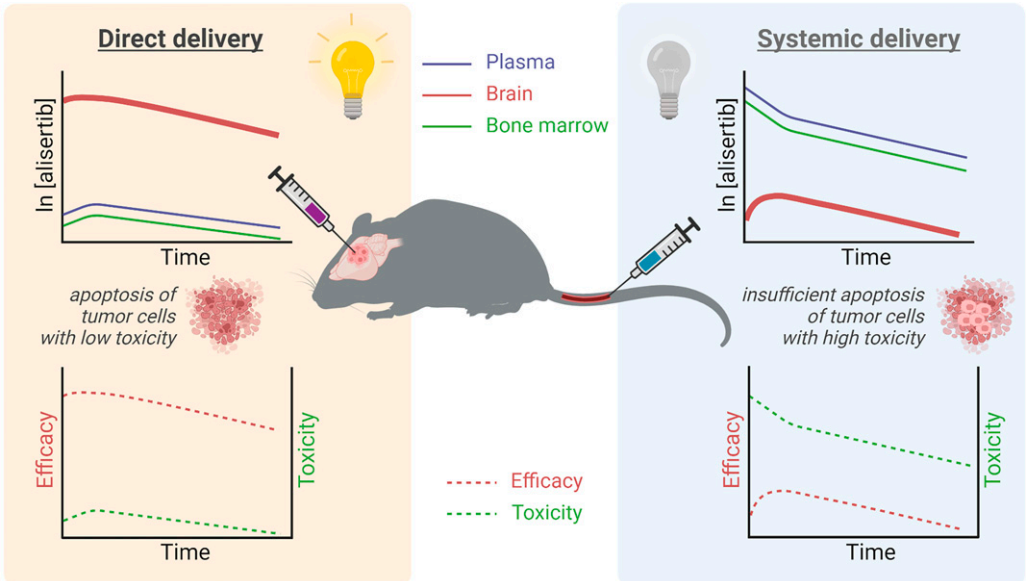

Fig. 8. Predicted exposure profiles of alisertib, efficacy, and toxicity in treatment of CNS tumors following direct and systemic delivery of alisertib (created with BioRender.com).

Downloaded from jpet.aspetjournals.org at ASPET Journals on April 17, 2024

excretion/secretion, indicating that the effect of transport by P-gp on the systemic exposure of alisertib would not be significant.

The inhibitory effect of elacridar on CNS distribution of alisertib was not observed after 0.25 hours post co-administration of alisertib and elacridar in wild-type mice. However, it was clearly shown to increase inhibitory effect after 1 hour post administration (Fig. 6, Table 5). The time to reach maximum concentration of elacridar in plasma is 1 hour after intraperitoneal injection. Considering that free plasma concentrations of elacridar are approximately 0.03 and 0.2 μM after 0.25 and 1 hour of intraperitoneal injection, respectively, the pharmacologically active concentration of elacridar may not be high enough to inhibit export of alisertib from the CNS after 0.25 hours post dose (Kallem et al., 2012; Sane et al., 2013a). The inhibitory potential of elacridar against efflux by P-gp varies depending upon the substrate, but to our knowledge, neither the IC_{50} nor the K_i of elacridar to inhibit the transport of alisertib by P-gp is known (Tang et al., 2002; Rautio et al., 2006).

Adverse events are one of the major determinants for the clinical application of investigational drugs. Therefore, the drug distribution into the site of toxicity as well as into the site of efficacy is necessary information to inform an appropriate dosage regimen that will optimize the therapeutic index in patients. One of the dose-limiting side effects of alisertib is myelosuppression. This has been observed with a high frequency where more than 40% of 249 patients experienced grade 3–4 myelosuppression during a phase II clinical trial (Melichar et al., 2015). The toxicity of alisertib was dose-related with a higher frequency in children than in adults (Dees et al., 2012; Mossé et al., 2012; Melichar et al., 2015; Lin et al., 2016). In this preclinical study, bone marrow concentrations of alisertib were comparable to plasma concentrations, which were similar in wild-type and P-gp knockout mice. Although it is known that P-gp exerts a barrier function in hematopoietic cells (Schinkel et al., 1997), its relative expression and function in bone marrow cells compared with the epithelium in the CNS is unclear. Moreover, free concentrations of alisertib in bone marrow were not available. Despite these limitations, our results, i.e., similar bone marrow K_p in wild-type and transgenic mice lacking P-gp, indicate that P-gp does not play a significant role in the bone marrow distribution of alisertib. Also, considering the similar pharmacokinetic profiles and comparable concentrations between bone marrow and plasma as shown in Fig. 7, the bone marrow concentrations of alisertib are predictable from plasma concentrations, allowing one to use the relationship between the systemic exposure and myelosuppression to help guide dosing.

Alisertib exhibited a promising therapeutic effect in glioblastoma cell lines with an IC_{50} in the range of 30–95 nM, the equivalent of 16–49 ng/ml (Kurokawa et al., 2017). If alisertib is administered systemically, and given the $K_{p,uu}$ we determined in the brain, the plasma concentrations of alisertib need to be at least 86 μg/ml to achieve an efficacious concentration in the brain. The human equivalent dose for 30 mg/kg in mice, one that improved survival in orthotopic glioblastoma models, is estimated to be approximately 170 mg/70 kg (Nair and Jacob, 2016). In patients, however, C_{max} of alisertib was approximately 2 μg/ml after a single oral dose of 150 mg and approximately 1.7 μg/ml after 50 mg of twice daily doses for 7 days (Dees et al., 2012), suggesting that a much higher dose than the clinical dose currently employed is required to reach the effective concentration for the treatment of CNS tumors. However, given that this high systemic exposure would result in a higher risk of side effects, especially myelosuppression, this dose is not clinically feasible. An alternative to a high systemic dose is a direct delivery method into the CNS that bypasses the BBB, such as convection-enhanced delivery (CED). This could be adopted to avoid high systemic exposure while maximizing availability of alisertib at the disease site. Importantly, if CED is to be utilized, the impact of active efflux on the mean transit time of alisertib at the tumor site needs to also be considered. This may result in either multiple or longer duration administration by CED.

In conclusion, we have shown that the CNS penetration of alisertib is limited with an equivalent distribution across several anatomic regions in the mouse CNS. Also, this study shows that P-gp, rather than Bcrp, plays a significant role in restricting CNS distribution of alisertib, and the influence of P-gp on brain distribution, as measured by the brain-to-plasma concentration ratio is uniform throughout the CNS regions studied. Moreover, to our knowledge, this is the first report to quantitatively determine the bone marrow distribution of alisertib over time. The concentration of alisertib in bone marrow rapidly becomes proportional to that in plasma. The bone marrow concentration is significantly higher than the CNS concentration, indicating that systemic exposure of alisertib may cause adverse events related to bone marrow suppression when treating patients with CNS tumors. Taken together, distribution of alisertib is low at the site of efficacy, the CNS, but high at the site of toxicity, the bone marrow in mice. These results warrant further investigation to secure an efficacious concentration in the CNS with low systemic exposure. Targeted delivery to the CNS (Fig. 8) could be utilized for this purpose.

Acknowledgments

The authors thank James Fisher (Clinical Pharmacology Analytical Services Laboratory, University of Minnesota) and Yingchun Zhao (Analytical Biochemistry, Masonic Cancer Center, University of Minnesota) for their help and support in the development and optimization of the LC-MS/MS analysis.

Authorship Contributions

Participated in research design: Oh, Power, Daniels, Elmquist.
Conducted experiments: Oh, Zhang.
Performed data analysis: Oh, Elmquist.
Wrote or contributed to the writing of the manuscript: Oh, Elmquist.

References

Agarwal S, Hartz AMS, Elmquist WF, and Bauer B (2011b) Breast cancer resistance protein and P-glycoprotein in brain cancer: two gatekeepers team up. *Curr Pharm Des* **17**:2793–2802.
Agarwal S, Sane R, Oberoi R, Ohlfest JR, and Elmquist WF (2011a) Delivery of molecularly targeted therapy to malignant glioma, a disease of the whole brain. *Expert Rev Mol Med* **13**:e17.
Agarwal S, Uchida Y, Mittapalli RK, Sane R, Terasaki T, and Elmquist WF (2012) Quantitative proteomics of transporter expression in brain capillary endothelial cells isolated from P-glycoprotein (P-gp), breast cancer resistance protein (Bcrp), and P-gp/Bcrp knockout mice. *Drug Metab Dispos* **40**:1164–1169.
Allen JD, Brinkhuis RF, Wijnholds J, and Schinkel AH (1999) The mouse Bcrp1/Mxr/Abcp gene: amplification and overexpression in cell lines selected for resistance to topotecan, mitoxantrone, or doxorubicin. *Cancer Res* **59**:4237–4241.
Amend SR, Valkenburg KC, and Pienta KJ (2016) Murine Hind Limb Long Bone Dissection and Bone Marrow Isolation. *J Vis Exp* **110**:53936.
Bailer AJ (1988) Testing for the equality of area under the curves when using destructive measurement techniques. *J Pharmacokinet Biopharm* **16**:303–309.
Banks WA (2016) From blood-brain barrier to blood-brain interface: new opportunities for CNS drug delivery. *Nat Rev Drug Discov* **4**:275–292.
Bolliger AP and Everds N (2012) Haematology of the mouse, in *The Laboratory Mouse* (Hedrich H, ed) pp 331–347.
Chavko M, Nemoto EM, and Melick JA (1993) Regional lipid composition in the rat brain. *Mol Chem Neuropathol* **18**:123–131.

Downloaded from jpet.aspetjournals.org at ASPET Journals on April 17, 2024

Chen Y, Agarwal S, Shaik NM, Chen C, Yang Z, and Elmquist WF (2009) P-glycoprotein and breast cancer resistance protein influence brain distribution of dasatinib. *J Pharmacol Exp Ther* **330**:956–963.
Chugh BP, Lerch JP, Yu LX, Pienkowski M, Harrison RV, Henkelman RM, and Sled JG (2009) Measurement of cerebral blood volume in mouse brain regions using micro-computed tomography. *Neuroimage* **47**:1312–1318.
Dai H, Marbach P, Lemaire M, Hayes M, and Elmquist WF (2003) Distribution of STI-571 to the brain is limited by P-glycoprotein-mediated efflux. *J Pharmacol Exp Ther* **304**:1085–1092.
Daniel WA, Wójcikowski J, and Pałucha A (2001) Intracellular distribution of psychotropic drugs in the grey and white matter of the brain: the role of lysosomal trapping. *Br J Pharmacol* **134**:807–814.
de Gooijer MC, Kemper EM, Buil LCM, Çitirikkaya CH, Buckle T, Beijnen JH, and van Tellingen O (2021) ATP-binding cassette transporters restrict drug delivery and efficacy against brain tumors even when blood-brain barrier integrity is lost. *Cell Reports Med* **2**:100184.
Dees EC, Cohen RB, von Mehren M, Stinchcombe TE, Liu H, Venkatakrishnan K, Manfredi M, Fingert H, Burris 3rd HA, and Infante JR (2012) Phase I study of aurora A kinase inhibitor MLN8237 in advanced solid tumors: safety, pharmacokinetics, pharmacodynamics, and bioavailability of two oral formulations. *Clin Cancer Res* **18**:4775–4784.
Eyal S, Ke B, Muzi M, Link JM, Mankoff DA, Collier AC, and Unadkat JD (2010) Regional P-glycoprotein activity and inhibition at the human blood-brain barrier as imaged by positron emission tomography. *Clin Pharmacol Ther* **87**:579–585.
Goos JACM, Verbeek J, Geldof AA, Hiemstra AC, van de Wiel MA, Adamzek KA, Delis-Van Diemen PM, Stroud SG, Bradley DP, Meijer GA et al. (2016) Molecular imaging of aurora kinase A (AURKA) expression: Synthesis and preclinical evaluation of radiolabeled alisertib (MLN8237). *Nucl Med Biol* **43**:63–72.
Griffith JI, Sarkaria JN, and Elmquist WF (2021) Efflux Limits Tumor Drug Delivery Despite Disrupted BBB. *Trends Pharmacol Sci* **42**:426–428.
Hill RM, Kuijper S, Lindsey JC, Petrie K, Schwalbe EC, Barker K, Boult JKR, Williamson D, Ahmad Z, Hallsworth A et al. (2015) Combined MYC and P53 defects emerge at medulloblastoma relapse and define rapidly progressive, therapeutically targetable disease. *Cancer Cell* **27**:72–84.
Hyafil F, Vergely C, Du Vignaud P, and Grand-Perret T (1993) In vitro and in vivo reversal of multidrug resistance by GF120918, an acridonecarboxamide derivative. *Cancer Res* **53**:4595–4602.
Kallem R, Kulkarni CP, Patel D, Thakur M, Sinz M, Singh SP, Mahammad SS, and Mandlekar S (2012) A simplified protocol employing elacridar in rodents: a screening model in drug discovery to assess P-gp mediated efflux at the blood brain barrier. *Drug Metab Lett* **6**:134–144.
Kalvass JC and Maurer TS (2002) Influence of nonspecific brain and plasma binding on CNS exposure: implications for rational drug discovery. *Biopharm Drug Dispos* **23**:327–338.
Kodaira H, Kusuhara H, Ushiki J, Fuse E, and Sugiyama Y (2010) Kinetic analysis of the cooperation of P-glycoprotein (P-gp/Abcb1) and breast cancer resistance protein (Bcrp/Abcg2) in limiting the brain and testis penetration of erlotinib, flavopiridol, and mitoxantrone. *J Pharmacol Exp Ther* **333**:788–796.
Kogiso M, Qi L, Braun FK, Injac SG, Zhang L, Du Y, Zhang H, Lin FY, Zhao S, Lindsay H et al. (2018) Concurrent Inhibition of Neurosphere and Monolayer Cells of Pediatric Glioblastoma by Aurora A Inhibitor MLN8237 Predicted Survival Extension in PDOX Models. *Clin Cancer Res* **24**:2159–2170.
Kurokawa C, Geekiyanage H, Allen C, Iankov I, Schroeder M, Carlson B, Bakken K, Sarkaria J, Ecsedy JA, D'Assoro A et al. (2017) Alisertib demonstrates significant antitumor activity in bevacizumab resistant, patient derived orthotopic models of glioblastoma. *J Neurooncol* **131**:41–48.
Lehman NL, O'Donnell JP, Whiteley LJ, Stapp RT, Lehman TD, Roszka KM, Schultz LR, Williams CJ, Mikkelsen T, Brown SL et al. (2012) Aurora A is differentially expressed in gliomas, is associated with patient survival in glioblastoma and is a potential chemotherapeutic target in gliomas. *Cell Cycle* **11**:489–502.
Lin J, Patel SA, Sama AR, Hoffman-Censits JH, Kennedy B, Kilpatrick D, Ye Z, Yang H, Mu Z, Leiby B et al. (2016) A Phase I/II Study of the Investigational Drug Alisertib in Combination with Abiraterone and Prednisone for Patients with Metastatic Castration-Resistant Prostate Cancer Progressing on Abiraterone. *Oncologist* **21**:1296–1297e.
Liow JS, Kreisl W, Zoghbi SS, Lazarova N, Seneca N, Gladding RL, Taku A, Herscovitch P, Pike VW, and Innis RB (2009) P-glycoprotein function at the blood-brain barrier imaged using 11C-N-desmethyl-loperamide in monkeys. *J Nucl Med* **50**:108–115.
Melichar B, Adenis A, Lockhart AC, Bennouna J, Dees EC, Kayaleh O, Obermannova R, DeMichele A, Zatloukal P, Zhang B et al. (2015) Safety and activity of alisertib, an investigational aurora kinase A inhibitor, in patients with breast cancer, small-cell lung cancer, non-small-cell lung cancer, head and neck squamous-cell carcinoma, and gastro-oesophageal adenocarcinoma: a five-arm phase 2 study. *Lancet Oncol* **16**:395–405.
Michaelis M, Selt F, Rothweiler F, Löschmann N, Nüsse B, Dirks WG, Zehner R, and Cinatl Jr J (2014) Aurora kinases as targets in drug-resistant neuroblastoma cells. *PLoS One* **9**:e108758.
Michaelis M, Selt F, Rothweiler F, Wiese M, and Cinatl Jr J (2015) ABCG2 impairs the activity of the aurora kinase inhibitor tozasertib but not of alisertib. *BMC Res Notes* **8**:484.
Mossé YP, Lipsitz E, Fox E, Teachey DT, Maris JM, Weigel B, Adamson PC, Ingle MA, Ahern CH, and Blaney SM (2012) Pediatric phase I trial and pharmacokinetic study of MLN8237, an investigational oral selective small-molecule inhibitor of Aurora kinase A: a Children's Oncology Group Phase I Consortium study. *Clin Cancer Res* **18**:6058–6064.
Mou PK, Yang EJ, Shi C, Ren G, Tao S, and Shim JS (2021) Aurora kinase A, a synthetic lethal target for precision cancer medicine. *Exp Mol Med* **53**:835–847.
Nair AB and Jacob S (2016) A simple practice guide for dose conversion between animals and human. *J Basic Clin Pharm* **7**:27–31.
Niu H, Manfredi M, and Ecsedy JA (2015) Scientific Rationale Supporting the Clinical Development Strategy for the Investigational Aurora A Kinase Inhibitor Alisertib in Cancer. *Front Oncol* **5**:189.
Nyúl-Tóth Á, Suciu M, Molnár J, Fazakas C, Haskó J, Herman H, Farkas AE, Kaszaki J, Hermenean A, Wilhelm I et al. (2016) Differences in the molecular structure of the blood-brain barrier in the cerebral cortex and white matter: an in silico, in vitro, and ex vivo study. *Am J Physiol Heart Circ Physiol* **310**:H1702–H1714.
Otto T and Sicinski P (2017) Cell cycle proteins as promising targets in cancer therapy. *Nat Rev Cancer* **17**:93–115.
Pusalkar S, Zhou X, Li Y, Cohen L, Yang JJ, Balani SK, Xia C, Shyu WC, Lu C, Venkatakrishnan K et al. (2020) Biotransformation Pathways and Metabolite Profiles of Oral [14 C]alisertib (MLN8237), an Investigational Aurora A Kinase Inhibitor, in Patients with Advanced Solid Tumors. *Drug Metab Dispos* **48**:217–229.
Qaiser MZ, Dolman DEM, Begley DJ, Abbott NJ, Cazacu-Davidescu M, Corol DI, and Fry JP (2017) Uptake and metabolism of sulphated steroids by the blood-brain barrier in the adult male rat. *J Neurochem* **142**:672–685.
Rautio J, Humphreys JE, Webster LO, Balakrishnan A, Keogh JP, Kunta JR, Serabjit-Singh CJ, and Polli JW (2006) In vitro p-glycoprotein inhibition assays for assessment of clinical drug interaction potential of new drug candidates: a recommendation for probe substrates. *Drug Metab Dispos* **34**:786–792.
Richner M, Jager SB, Siupka P, and Vaegter CB (2017) Hydraulic Extrusion of the Spinal Cord and Isolation of Dorsal Root Ganglia in Rodents. *J Vis Exp* **2017**:55226.
Sane R, Agarwal S, Mittapalli RK, and Elmquist WF (2013b) Saturable active efflux by p-glycoprotein and breast cancer resistance protein at the blood-brain barrier leads to nonlinear distribution of elacridar to the central nervous system. *J Pharmacol Exp Ther* **345**:111–124.
Sane R, Mittapalli RK, and Elmquist WF (2013a) Development and evaluation of a novel microemulsion formulation of elacridar to improve its bioavailability. *J Pharm Sci* **102**:1343–1354.
Sarkaria JN, Hu LS, Parney IF, Pafundi DH, Brinkmann DH, Laack NN, Giannini C, Burns TC, Kizilbash SH, Laramy JK et al. (2018) Is the blood-brain barrier really disrupted in all glioblastomas? A critical assessment of existing clinical data. *Neuro-oncol* **20**:184–191.
Schinkel AH, Mayer U, Wagenaar E, Mol CAAM, van Deemter L, Smit JJM, van der Valk MA, Voordouw AC, Spits H, van Tellingen O et al. (1997) Normal viability and altered pharmacokinetics in mice lacking mdr1-type (drug-transporting) P-glycoproteins. *Proc Natl Acad Sci USA* **94**:4028–4033.
Sells TB, Chau R, Ecsedy JA, Gershman RE, Hoar K, Huck J, Janowick DA, Kadambi VJ, LeRoy PJ, Stirling M et al. (2015) MLN8054 and Alisertib (MLN8237): Discovery of Selective Oral Aurora A Inhibitors. *ACS Med Chem Lett* **6**:630–634.
Smith DA, Di L, and Kerns EH (2010) The effect of plasma protein binding on in vivo efficacy: misconceptions in drug discovery. *Nat Rev Drug Discov* **9**:929–939.
Söderberg M, Edlund C, Kristensson K, and Dallner G (1990) Lipid compositions of different regions of the human brain during aging. *J Neurochem* **54**:415–423.
Tang F, Horie K, and Borchardt RT (2002) Are MDCK cells transfected with the human MDR1 gene a good model of the human intestinal mucosa? *Pharm Res* **19**:765–772.
Treyer A, Mateus A, Wiśniewski JR, Boriss H, Matsson P, and Artursson P (2018) Intracellular Drug Bioavailability: Effect of Neutral Lipids and Phospholipids. *Mol Pharm* **15**:2224–2233.
Vagiannis D, Zhang Y, Budagaga Y, Novotna E, Skarka A, Kammerer S, Küpper JH, and Hofman J (2022) Alisertib shows negligible potential for perpetrating pharmacokinetic drug-drug interactions on ABCB1, ABCG2 and cytochromes P450, but acts as dual-activity resistance modulator through the inhibition of ABCC1 transporter. *Toxicol Appl Pharmacol* **434**:115823.
Weiss N, Miller F, Cazaubon S, and Couraud PO (2009) The blood-brain barrier in brain homeostasis and neurological diseases. *Biochim Biophys Acta* **1788**:842–857.
Wen Z, Huang Y, Behler N, Bambal R, Bhoopathy S, and Owen A(2010) Determination of red blood cell partitioning and whole blood to plasma ratio using human, rat, and mouse blood: methods, model compounds and species diffferences, Poster W4305 at the *AAPS 2010 Annual Meeting*.
Wu G, Broniscer A, McEachron TA, Lu C, Paugh BS, Becksfort J, Qu C, Ding L, Huether R, Parker M et al.; St. Jude Children's Research Hospital–Washington University Pediatric Cancer Genome Project (2012) Somatic histone H3 alterations in pediatric diffuse intrinsic pontine gliomas and non-brainstem glioblastomas. *Nat Genet* **44**:251–253.
Yang JJ, Li Y, Chakravarty A, Lu C, Xia CQ, Chen S, Pusalkar S, Zhang M, Ecsedy J, Manfredi MG et al. (2014) Preclinical drug metabolism and pharmacokinetics, and prediction of human pharmacokinetics and efficacious dose of the investigational Aurora A kinase inhibitor alisertib (MLN8237). *Drug Metab Lett* **7**:96–104.
You D, Shin HM, Mosaad F, Richardson JR, and Aleksunes LM (2019) Brain region-specific regulation of histone acetylation and efflux transporters in mice. *J Biochem Mol Toxicol* **33**:e22318.
Youdim KA, Qaiser MZ, Begley DJ, Rice-Evans CA, and Abbott NJ (2004) Flavonoid permeability across an in situ model of the blood-brain barrier. *Free Radic Biol Med* **36**:592–604.
Yuan J (1993) Estimation of variance for AUC in animal studies. *J Pharm Sci* **82**:761–763.
Zhang L, Bender A, and Daniels D (2018) DIPG-21. Evaluating therapeutic vulnerabilities in DIPG using Aurora kinase inhibitor as a noverl therapy. *Neuro-oncol* **20**:i53.

Address correspondence to: Ju-Hee Oh, Department of Pharmaceutics, College of Pharmacy, University of Minnesota, 308 Harvard ST SE, Minneapolis MN 55455. E-mail: oh000074@umn.edu; or William F. Elmquist, Department of Pharmaceutics, College of Pharmacy, University of Minnesota, 308 Harvard ST SE, Minneapolis MN 55455. E-mail: elmqu011@umn.edu

Downloaded from jpet.aspetjournals.org at ASPET Journals on April 17, 2024